IEEE Access
Multidisciplinary ⋮ Rapid Review ⋮ Open Access Journal

Received December 30, 2020, accepted January 10, 2021, date of publication January 20, 2021, date of current version January 27, 2021.

Digital Object Identifier 10.1109/ACCESS.2021.3053171

Decoupled PI Controllers Based on Pulse-Frequency Modulation for Current Sharing in Multi-Phase LLC Resonant Converters

MARTIN MORENO[1], (Student Member, IEEE), JAVIER PEREDA[2,3], (Member, IEEE), FELIX ROJAS[4], (Member, IEEE), AND IVAN DOMINGUEZ-LOPEZ[5]

[1]Mechatronics Group, Centro de Investigación en Ciencia Aplicada y Tecnología Avanzada, Instituto Politécnico Nacional, Querétaro 76090, México
[2]Department of Electrical Engineering, Pontificia Universidad Católica de Chile, Santiago 7820436, Chile
[3]UC Energy Research Center, Pontificia Universidad Católica de Chile, Santiago 7820436, Chile
[4]Department of Electrical Engineering, Universidad de Santiago de Chile, Santiago 9170022, Chile
[5]Materials Processing and Manufacturing Group, Centro de Investigación en Ciencia Aplicada y Tecnología Avanzada, Instituto Politécnico Nacional, Querétaro 76090, México

Corresponding author: Javier Pereda (jepereda@ing.puc.cl)

This work was supported in part by the ANID under Grant ANID/PIA/ACT192013, Grant ANID/FONDEF/ID20I10267, and Grant ANID/FONDAP/15110019 (SERC Chile). The work of Martin Moreno was supported in part by the Scholarship of Alianza del Pacífico, Secretaría de Investigación y Posgrado del Instituto Polítecnico Nacional (SIP-IPN), and in part by the CONACYT-México under Grant CVU-668623.

ABSTRACT The LLC series resonant converter has emerged as a solution to applications requiring power conversion with isolation, reduced volume and high efficiency, such as PV systems and EV chargers. However, the LLC resonant converter is limited in power, so it requires a multi-phase configuration in order to provide higher currents. This configuration connects the outputs of two or more LLC converters in parallel, increasing the output current but introducing imbalance and circulating currents due to the mismatch and tolerance values of components in each resonant tank. This paper proposes a simple PI control scheme to compensate the current imbalance and eliminate circulating currents generated when several LLC resonant converters are connected in parallel. Unlike reported current sharing methods, the proposed control scheme is based on multiple current control loops operating independently, using the switching frequency of each parallel-connected unit as a degree of freedom of the overall converter. The proposed control scheme has been successfully validated under simulations and experimental assessment, implementing two resonant tanks with ±5% tolerance of parameters, providing excellent steady-state and transient performance.

INDEX TERMS Current sharing, imbalance current, multi-phase LLC resonant converter, pulse-frequency modulation.

I. INTRODUCTION

High frequency isolated DC-DC converters offer high power density due to small transformers, inductors and capacitors, and have been successfully implemented in trending applications where isolation and high power density is relevant, such as photovoltaics [1]–[4], DC distribution grid [5]–[7] and EV chargers [8]–[10]. Due to the high switching frequency operation of these converters, soft switching techniques are implemented through special modulations algorithms or resonant tank circuits to reduce switching power losses [11]–[14].

The associate editor coordinating the review of this manuscript and approving it for publication was Zhilei Yao.

The multi-phase LLC resonant converter arises as an attractive and simple solution for achieving high efficiency, high power density and small footprint for DC/DC conversion [15]–[17]. Each phase of the multi-phase LLC resonant converter is composed of a front to front connection of an inverter and a non-controlled rectifier, linked by a medium or high frequency transformer and an LLC series resonant tank, as shown in Figure 1. The LLC resonant converter operates as a current source, so a class-D current-driven bridge rectifier with a capacitor filter is used. The converter achieves zero-voltage switching (ZVS) on the primary side inverter and zero-current switching (ZCS) on the secondary side rectifier when it operates around the resonant frequency of the LLC resonant tank. The LLC converter can

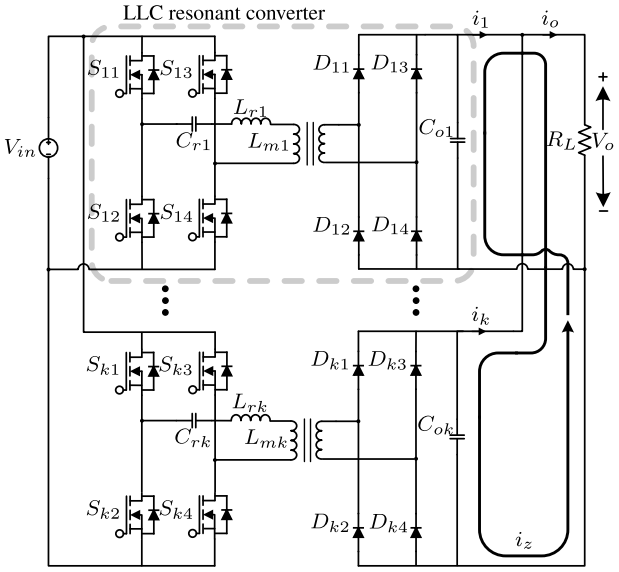

FIGURE 1. Multi-phase LLC resonant converter topology.

regulate the output current by adjusting: a) the duty cycle through phase-shift modulation (PSM); b) the input dc voltage through a power factor corrector (PFC); or c) the switching frequency through pulse frequency modulation (PFM).

The LLC converter is restricted in power due to nominal current and power losses capability in semiconductors and power rate limitations on medium or high frequency transformers (usually available for a couple of kVA) [18], [19]. At high frequency, the transformer core material should be soft magnetic material: ferrite, amorphous alloy or nanocrystalline. The first one has low saturation flux and the others can be too expensive for some commercial applications [19]. Additionally, the parasitic inductances and capacitances acquire more relevance at high frequency, affecting the performance, efficiency, and operation of the transformer. Thus, for high power applications such as fast EV chargers or string PV converters, multi-phase (parallel connected) LLC configurations are required, as shown in Figure 1. In the multi-phase configuration, each LLC resonant converter is manufactured to ideally provide an identical resonant frequency. However, a mismatch on electrical parameters among the different units is unavoidable, leading to a slightly different resonant frequency on LLC resonant converter. These small differences in resonance frequencies can cause serious problems, introducing high circulating currents and unbalancing the current distribution among the parallel-connected LLC resonant converters. Different solutions have been presented to balance the output currents and reduce circulating current, known as current sharing methods, which can be categorized into three main methods: a) passive current sharing; b) active current sharing and c) closed-loop control sharing method.

Passive current sharing methods equalize the impedance of all resonant tanks using passive elements. In [16] variable inductors are used to match the tank impedances among the resonant converters. Other methods interconnect the resonant tanks or transformers to change and match the equivalent impedance of each resonant converter [16], [20]–[22]. Additionally, it is possible to add a magnetic coupling to transfer energy between tanks, maintaining the same current amplitude for all tanks and a balanced operation [7], [23], [24]. However, these methods are complex, costly and bulky, have slow dynamic performance and do not maintain an even power distribution among all the units for the entire operating range.

Active current sharing methods compensate the mismatch of electrical parameters in the resonant tanks by adding extra power semiconductors devices and passive elements [25], [26]. Thus, the additional semiconductors devices regulate the current which flows through passive elements until the current reaches the resonance frequency [25], [26]. Although these methods are effective, they increase power losses due to the hard switching of the additional semiconductor devices and reduce the power density of the overall converter by incorporating additional passive elements, increasing the cost and reducing the reliability [26].

Closed-loop control schemes have been proposed as an effective alternative to achieve current sharing in multi-phase LLC resonant converters. These methods use modulation strategies to control each primary side inverter independently and balance the output currents. The closed-loop control schemes govern the output current of each LLC converter to reduce the difference between them, providing balanced currents at a steady-state performance. These control schemes can be classified into centralized-loop control and master-slave control strategy. The centralized-loop controls use the output currents of other LLC converters to balance the currents through PFM or interleave modulation with phase-shift in each half-bridge. However, this control scheme introduces a permanent error in the current sharing due to the response time of other converters [27]–[31]. On the other hand, the master-slave strategy has been proposed to interleave the LLC converters and tracking the master-unit frequency, improving the steady-state error of current sharing, but the control reliability is reduced due to complete dependence on the master control and the communication bus [15], [32]–[34]. Both control schemes use master or centralized controllers, which reduce the modularity and increase the complexity due to their coupled behavior, resulting in complicated tuning processes every time a parallel converter is added [8]. Modular control for multi-phase LLC resonant converter should be easier to scale up without requiring complex retuning processes and keeping a low steady-state balance error.

This paper presents a current sharing method using independent current loops for each LLC converter, which shows a suitable dynamic transition under variation of the reference current and the ability to compensate load disturbances. The proposed solution stands out for its simplicity, and as far as the authors know, it has not been addressed in other works,

since there are other papers that use frequency control in LLC converters, but none of them perform it independently or analyze the circulating currents under independent modulations [15], [29]–[34].

Each control loop consists of a linear current regulator that manipulates the converter frequency around the resonant frequency through a pulse-frequency modulator (PFM). The gains of linear regulators are tuned with the ideal-parameters of the nominal LLC filter, so the gains have the same value for all regulators, keeping the modularity and the current sharing despite the mismatch of the parameter. Unlike reported methods, the proposed decoupled control scheme reduces circulating currents and provides a balanced current distribution among all parallel-connected LLC resonant converters with a simple and decoupled tuning of each controller. Therefore, the proposed control method can be directly extended to any number of parallel-connected units.

The rest of this paper is structured into five sections. Section II presents the operation of the LLC resonant converter and a circulating current analysis for different modulation techniques. Section III shows the proposed control scheme for the multi-phase LLC resonant converter. Finally, section IV and V show the experimental results and conclusions accordingly.

II. OPERATION OF MULTI-PHASE LLC RESONANT CONVERTER

This section first presents a model of the LLC converter and then analyzes the circulating current according to three modulation techniques, excluding the control.

A. MODELING OF LLC RESONANT CONVERTER

From Figure 1, the resonant frequency (f_{rk}) and bandwidth for the k^{th} LLC resonant converter is determined by the transformer resonant capacitor (C_{rk}), the resonant inductor (L_{rk}) and the magnetizing inductance (L_{mk}) integrated in the transformer. Each full-bridge generates a square-waveform voltage with a switching frequency f_{sk}, supplying the resonant tank and generating a resonant current that feeds the transformer.

Considering the k^{th} LLC resonant converter, the impedance of its resonant tank can be analyzed by its equivalent circuit and it is linked to the voltage gain model as presented in (1) [35]. This model shows critical operation points in terms of the normalized frequency (f_{nk}) and describes different operation regions where the LLC converter keeps the soft-switching.

$$\frac{V_o}{V_{in}} = \frac{f_{nk}^2(m_k-1)}{\sqrt{(m_k\cdot f_{nk}^2-1)^2+f_{nk}^2\cdot Q_k^2(f_{nk}^2-1)^2(m_k-1)^2}} \tag{1}$$

The equivalent load (R_{ok}) is defined as:

$$R_{ok} = \frac{8}{\pi^2}\frac{V_o}{I_o} = \frac{8}{\pi^2}n_k^2 R_L \tag{2}$$

where n_k is the transformer ratio, $m_k = (L_{rk}+L_{mk})/L_{rk}$ is the inductance ratio, $Q_k = 1/R_{ok}\sqrt{L_{rk}/C_{rk}}$ is the quality factor, $f_{nk} = f_{sk}/f_{rk}$ is the normalized frequency, and the resonant frequency is expressed as:

$$f_{rk} = \frac{1}{2\pi\sqrt{L_{rk}C_{rk}}} \tag{3}$$

The voltage-gain model in (1) associates the losses of the tank with the load (R_L). The tank losses are bounded by the minimum and maximum normalized frequency, which are illustrated in Figure 2. The minimum frequency is determined by the impedance tank [35], and the maximum frequency is defined by the impedance tank and the dead time [36].

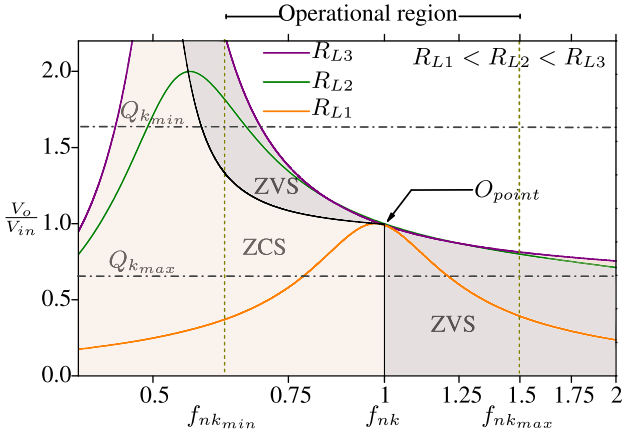

FIGURE 2. Voltage-gain model for LLC resonant converter under different load conditions, $R_{L1} < R_{L2} < R_{L3}$.

An external voltage control-loop was not considered in this paper due to it depends on the application, and even more, some of them use only current controllers, such as the fast battery charger in CC mode, or a photovoltaic converter with an MPPT based on current reference. Therefore, a relation between the output current (i_k) and the switching frequency (f_{sk}) of the k^{th} converter can be obtained from Appendix B as:

$$G_{if_k}(s) = \frac{i_k(s)}{f_{sk}(s)} = \frac{k_{fk}(sC_{ok}+\frac{1}{R_L})}{s^2\frac{L_{eqk}C_{ok}}{n_k^2}+s\frac{L_{eqk}}{n_k^2R_L}+1} \tag{4}$$

$$k_{fk} = -\frac{8}{n_k\pi}\frac{L_{mk}}{L_{rk}}\frac{1}{f_{rk}}V_{in} \tag{5}$$

$$L_{eqk} \approx \frac{\pi^2}{4}L_{rk} \tag{6}$$

The gain k_{fk} comes from the maximization of the voltage-gain model (1), respect to the resonance frequency after partial derivation. The L_{eqk} is defined as the equivalent impedance of the tank at the resonant frequency. The i_k of the transfer function (4) is affected by C_{ok}, L_{eqk} and n_k, which were used in the experiments (section IV) with variations of $\pm 0.5\%$, $\pm 5\%$ and $\pm 10\%$, respectively. C_{ok}, L_{eqk} and n_k have a linear correlation of 0.2, -0.39 and 0.43 with the i_k at the resonant frequency (f_{rk}). Therefore, n_k has more impact to i_k than C_{ok} and L_{eq} has a negative correlation, which means L_{eqk} influences in lower proportion the i_k.

Figure 2 shows the operational region of the LLC converter for different loads. The best operation point for the efficiency near the resonant frequency at the O_{point}, where the converter has no dependency of the load (R_L) and achieves ZVS on the primary side and ZCS on the secondary side. However, changes in R_L imply variations in the voltage gain and the dynamic. Therefore, the normalized frequency f_{nk} must be controlled under a bandwidth according to the application. As an example, the LLC converter can be applied as a fast battery charger, following a constant current (CC) profile, which requires control of f_{nk} due to the variation of Q_k, as is detailed in [37] as follows: i) at the beginning, the battery is totally discharged and the LLC converters will start at its maximum operational frequency f_{max}; ii) then, the frequency will go gradually down to keep a constant current while the battery voltage increases; iii) finally, the battery reaches its maximum voltage and the fast charging finishes at its minimum operational frequency f_{min}. All the previous processes are made at constant current (CC), following the output current reference i_o^* from the Battery Management System (BMS).

The multi-phase LLC converter has imbalances and circulating current, which increases the stress and power losses in the converter. Additionally, the circulating current is highly sensitive to the modulation applied. For this reason, the phase and frequency of the modulation must be analyzed.

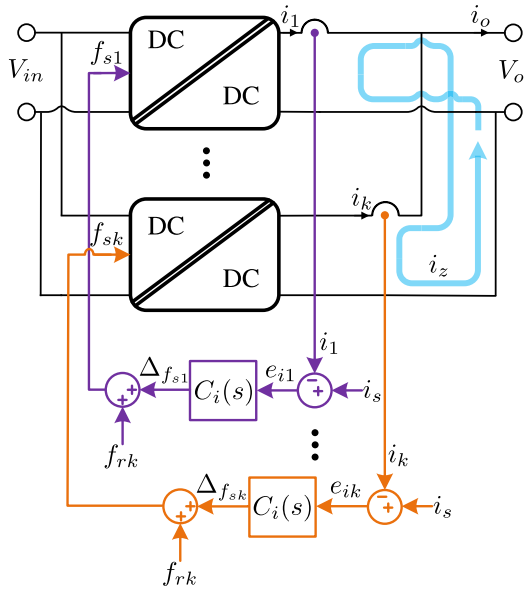

FIGURE 3. Control scheme of multi-current control loop for multi-phase LLC resonant converter.

B. CIRCULATING CURRENTS OF MULTI-PHASE LLC CONVERTER

The circulating current (i_z) is generated by the difference between the output currents of each LLC resonant converter and circulates among the output capacitors and rectifiers (Figure 3). On the other hand, the output current (i_o) is the sum of each output current and goes directly to the load. Considering two parallel-connected converters for simplicity, i_o and i_z can be expressed as:

$$i_o = i_1 + i_2 \tag{7}$$

$$i_z = i_1 - i_2 \tag{8}$$

The circulating current is highly sensitive to the resonant impedance tank and the modulation implemented. Thereby, any mismatch on magnitude, frequency or phase on the output currents will lead to circulating currents. The dc component of the circulating current ($\bar{i}_z$) depends on the resonant tank mismatch, and the ac component ($\tilde{i}_z$) is related to the modulation implemented. The dc component of circulating current is eliminated by the closed-loop control to balance the output currents, which is proposed in the next section and it is not part of the modulation analyses presented in this section. Therefore, this section focuses on the modulation impact, so only the ac component will be analyzed. Then, the fundamental ac component of the output of each converter ($\tilde{i}_k^{\,1}$) can be written as:

$$\tilde{i}_1^{\,1} = I_1 \cdot \sin(2\omega_1 t + \phi_1) \tag{9}$$

$$\tilde{i}_2^{\,1} = I_2 \cdot \sin(2\omega_2 t + \phi_2) \tag{10}$$

Each converter can generate an ac component of the output current with different frequency, magnitude and phase, which depends mainly on the modulation technique implemented. Due to the rectification process, the fundamental frequency on each output current is twice the frequency of the resonant tank current. The higher even harmonics can be neglected due to their low amplitude and the filtering action of the output capacitor. Three different modulation techniques are analyzed to study the ac circulating currents phenomena: 1) twin modulation; 2) interleave modulation; and 3) pulse-frequency modulation (PFM).

1) TWIN MODULATION

This modulation operates each LLC resonant converters with an identical square-waveform, at the same frequency ($\omega_1 = \omega_2$) and phase ($\phi_1 = \phi_2$). However, the current amplitudes I_1 and I_2 can be different due to resonant parameters mismatch. Therefore, the ac component of the output and circulating current are:

$$i_o = \overbrace{(I_1 + I_2) \cdot \sin(2\omega_1 t + \phi_1)}^{\tilde{i}_o} + \overbrace{(\bar{I}_1 + \bar{I}_2)}^{\bar{i}_o} \tag{11}$$

$$i_z = \underbrace{(I_1 - I_2) \cdot \sin(2\omega_1 t + \phi_1)}_{\tilde{i}_z} + \underbrace{(\bar{I}_1 - \bar{I}_2)}_{\bar{i}_z} \tag{12}$$

Thus, the resonant tank mismatch between the LLC converters not only affects the average value of the circulating current, but it is also proportional to its ac component. On the other hand, the ac component of the output current is independent of the current sharing (or current difference) and cannot be reduced.

2) INTERLEAVE MODULATION

This modulation operates the LLC converters with square-waves at the same frequency ($\omega_2 = \omega_1$) but shifted

in π/k, generating in this case $\phi_2 = \phi_1 + \pi$ due to the rectifier doubles the frequency. Then, the ac component of the output and circulating current are:

$$\widetilde{i_o} = (I_1 - I_2) \cdot \sin(2\omega_1 t + \phi_1) \quad (13)$$

$$\widetilde{i_z} = (I_1 + I_2) \cdot \sin(2\omega_1 t + \phi_1) \quad (14)$$

Therefore, the interleave modulation behaves inversely to the twin modulation, because the resonant tank mismatch affects the output current ripple, which is eliminated only if $I_1 = I_2$. And the ac component of the circulating current is independent of the current sharing and cannot be reduced.

3) PULSE-FREQUENCY MODULATION (PFM)

This modulation operates each LLC resonant converter with square-wave at a different frequency and no relation is given for ϕ_1 and ϕ_2. Thus, circulating and output current are:

$$\widetilde{i_o} = I_1 \sin(2\omega_1 t + \phi_1) + I_2 \sin(2\omega_2 t + \phi_2) \quad (15)$$

$$\widetilde{i_z} = I_1 \sin(2\omega_1 t + \phi_1) - I_2 \sin(2\omega_2 t + \phi_2) \quad (16)$$

These ac currents cannot be easily analyzed as in the previous modulations. However, assuming the current sharing is achieved by some method (passive, active or closed-loop control), then the dc circulating current would be zero ($\overline{i_z} = 0$) and $I = I_1 = I_2$. Therefore, the circulating and output currents could be expressed as:

$$\widetilde{i_o} = 2I \cdot \sin\left((\omega_1 + \omega_2)t + \frac{\phi_1 + \phi_2}{2}\right) \cdot \cos\left(\Delta\omega t + \frac{\Delta\phi}{2}\right) \quad (17)$$

$$\widetilde{i_z} = 2I \cdot \sin\left(\Delta\omega t + \frac{\Delta\phi}{2}\right) \cdot \cos\left((\omega_1 + \omega_2)t + \frac{\phi_1 + \phi_2}{2}\right) \quad (18)$$

The ac component of the circulating and output currents can not be eliminated, even when $I_1 = I_2$. However, the ac components of both current is a trade-off between the twin and interleave modulations, obtaining a lower effective value of $\widetilde{i_o}$ than twin modulation and a lower average $\widetilde{i_z}$ than the interleave modulation. The circulating current waveform is a high-frequency signal at $\omega_1 + \omega_2$, with amplitude modulation at a lower frequency at $\Delta\omega = \omega_1 - \omega_2$. The figure 6 is clearly seen the waveform of the equation (17) and (18).

III. PROPOSED MULTI-CURRENT CONTROL LOOP FOR MULTI-PHASE LLC RESONANT CONVERTER

A multi-current PI control loop, formed by one independent linear controller for each LLC converter, is proposed and shown in Figure 3. Each PI controller regulates the DC component of the output current for each LLC converter. The current loops are set with an identical set-point current ($i_s = i_o^*/k$), where i_o^* comes from the high-level control of the application, such as from the BMS in a fast battery charging application. This forces each DC/DC converter to deliver an equally distributed portion of i_o, supplying an equal distribution of power.

Each PI controller $C_i(s)$ regulates an independent switching frequency (f_{sk}) for each LLC converter. Thereby, $C_i(s)$ delivers a shifting value Δ_{fsk} to actively adapt the individual frequency around the nominal resonant frequency f_{rk}, achieving accurate current sharing. The second-order transfer function G_{ifk} (4) relates the controlled output current with the actuation variable f_{sk}. This transfer function is used to design each PI controller $C_i(s)$ of Figure 3.

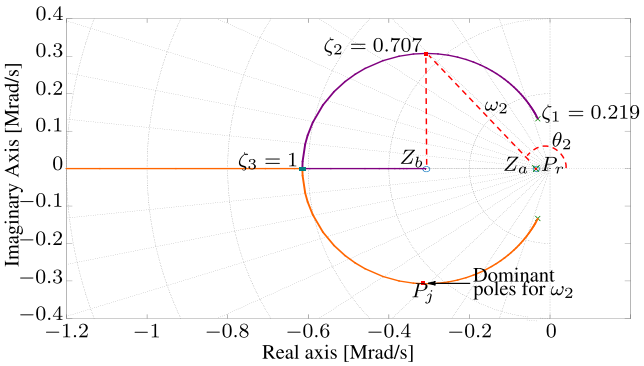

FIGURE 4. Root locus of current loop and nominal LLC resonant converter. ω_k = 1.07Mrad/s, ζ_k = 0.502 & M_p = 16.1%.

TABLE 1. Experimental parameters of multi-phase LLC resonant converter.

Variable	LLC_N	LLC_1	LLC_2
L_{rk}	230 μH	221 μH	243 μH
L_{mk}	371 μH	388 μH	355 μH
C_{rk}	33 nF	33.2 nF	33.4 nF
n_k	2	2.3	1.9
C_{ok}	20 μF	19.9 μF	21.1 μF
V_{in}	60 V	60 V	60 V
f_{rk}	57.7 kHz	58.7 kHz	55.9 kHz

Figure 4 shows the root locus diagram of the system composed of the controller $C_i(s)$ and the system plant G_{ifk}, where ideal parameters of the LLC resonant filter of Table 1 were used. Thus, the required natural frequency ω_k and damping coefficient ζ_k can be achieved by selecting the gains for each PI controller $C_i(s)$. In a real implementation, this procedure can be implemented independently for each of the k^{th} controllers of Figure 3, using different parameters for each LLC resonant filter. An analytical expression for each zero and pole of the root-locus plot can be found in Appendix C.

Nonetheless, for simplicity only ideal values of the LLC resonant filter can be considered to design a single PI controller and implement it in each independent control loop. This approach avoids the complex individual tuning process of each controller, improving modularity, flexibility, and power scalability, compared to existing solutions. Besides, considering that a proper design of passive components ensures small mismatches, only a negligible difference on transient response is compromised, without affecting the steady-state performance. In the case of experimental parameters of multi-phase LLC resonant converter, the difference in overshoot was 7.28%, the damping factor was 0.129, and the natural frequency was 33 krad/s.

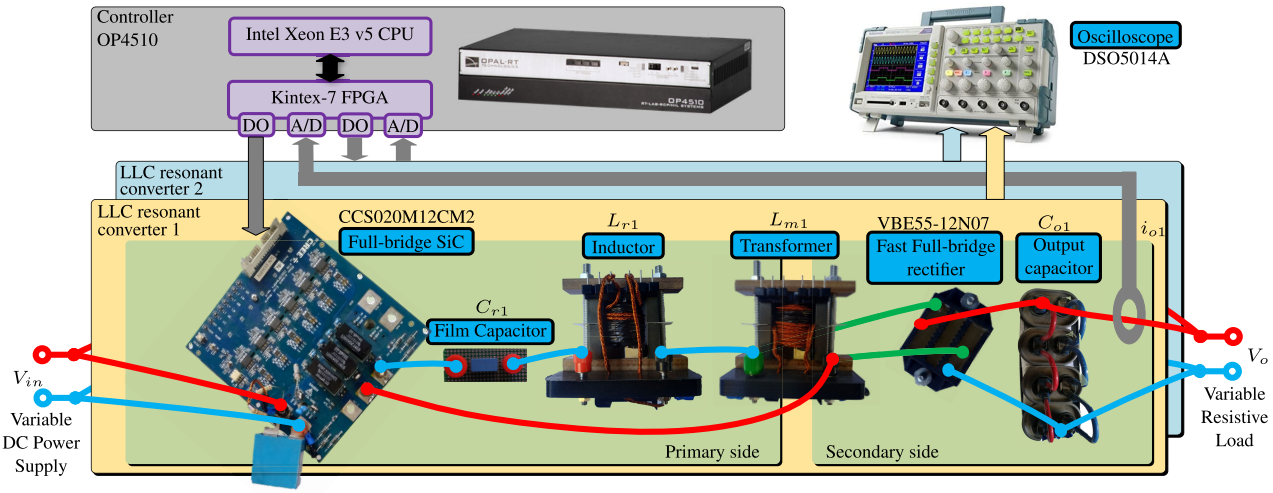

FIGURE 5. Multi-phase LLC converter prototype.

The PI controllers can work satisfactorily in a wide range of frequencies (30-230 kHz). However, the operational bandwidth in a real application would be much narrower due to the converter is designed to operate near the resonance frequency [37]. Following the example of the fast battery charger in section II, the proposed converter would work between 44-69 kHz during fast charging, assuming the battery varies between 380-500 V throughout the time of the CC range mode. The operation of the proposed control was evaluated in the following section for a wide frequency range, experimentally and in simulations.

IV. EXPERIMENTAL ASSESSMENT

To validate the proposed multi-current control loop for multi-phase LLC converters, and to support the output and circulating current analysis presented in section II, an experimental setup with two LLC resonant converters was implemented using two resonant tanks designed with ±5% mismatch on its parameters. The experimental setup was operated under the three different modulation techniques presented in section II (twin, interleave and PFM) to obtain experimental results that support previous analysis.

A. EXPERIMENTAL SETUP

Figure 5 shows the implemented experimental setup. It is composed of two LLC resonant converters connected in parallel. To mismatch the impedances, the resonant inductor, and transformer were first theoretically designed according to Appendix A. Theoretical design and practical implementation performed an accuracy of 98%. Capacitors, C_{r1} and C_{r2} preserve manufacture value (B32672L). Table 1 presents the values of all parameters used in the LLC converters.

The controlled inverter is composed of the SiC inverter module (CCS020M12CM2) triggered by the gate diver boards (CGD15FB45P1). The control and modulation of each LLC converter were implemented in the OPAL-RT platform OP4510. The secondary rectifier was composed of full-bridges fast diodes (VBE55-12N07), output capacitors (Z97F5339) and a R_L of 1.4Ω.

B. EXPERIMENTAL RESULTS

The experimental results of Figure 6 show the proposed controller with its pulse-frequency modulation (PFM) in comparison with the twin and interleave modulations described in section II. The left column of Figure 6 shows the currents under twin modulation, where both LLC converters have identical square-waves at 59 kHz. The central column of Figure 6 exhibits the currents under interleave modulation, where the square-waves also operate at 59 kHz but with a phase shift of $\pi/2$. Finally, the right column of Figure 6 presents the currents of the proposed multi-current loop with pulse-frequency modulation. As was analyzed in section II, the twin modulation has the lowest peak-to-peak circulating current $\widetilde{i_z}$ and it is proportional to the output current difference $(I_1 - I_2)$. While the interleave modulation has the highest circulating current ripple $\widetilde{i_z}$, independently of the current mismatch. However, interleave modulation has the lowest output current ripple $\widetilde{i_o}$ because ripple cancellation is proportional to $I_1 - I_2$.

The proposed control with PFM achieves current sharing ($\bar{i_z} = 0$) as well as supplies the same output current as other modulations. Therefore, the circulating current is composed only by the ac component ($i_z = \widetilde{i_z}$). This current has a high-frequency component equal to the sum of the LLC converter working frequencies $\omega_1 + \omega_2$, and a low-frequency component equal to $\omega_1 - \omega_2$, as presented in (18). The ripple of the output current ($\widetilde{i_o}$) is similar to the twin modulation, but the peak current in the rectifiers i_{rec} is very low and evenly distributed between both LLC converters. Therefore, the PFM reduces the stress on power devices and distributes the power losses evenly thanks to the multi-current control loop. It is important to notice that to achieve this, each PI

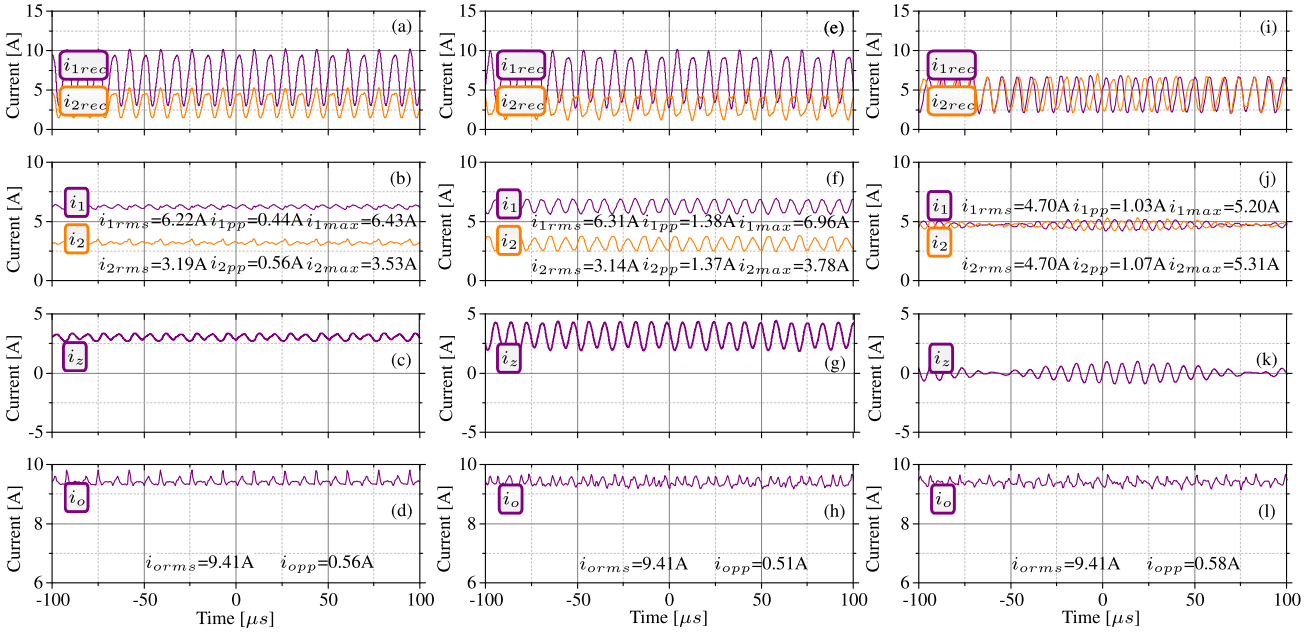

FIGURE 6. Experimental results of twin modulation. a) The rectified currents of first i_{1rec} and second i_{2rec} LCC converter. b) The output currents of first i_1 and second i_2 LLC converter. c) The circulating current i_z. d) The output current i_o of the multi-phase LLC resonant converter. Experimental results of interleave modulation. e) The rectified currents of first i_{1rec} and second i_{2rec} LCC converter. f) The output currents of first i_1 and second i_2 LLC converter. g) The circulating current i_z. h) The output current i_o of the multi-phase LLC resonant converter. Experimental results of PFM. i) The rectified currents of first i_{1rec} and second i_{2rec} LCC converter. j) The output currents of first i_1 and second i_2 LLC converter. k) The circulating current i_z. l) The output current i_o of the multi-phase LLC resonant converter.

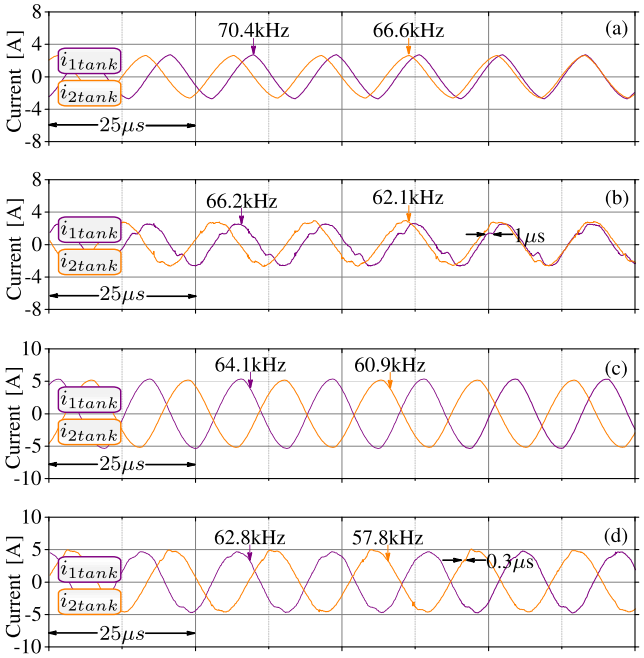

FIGURE 7. Resonant tank currents of the multi-phase LLC resonant converters in steady state. a) Simulation results at $i_s = 3$ A. b) Experimental results at $i_s = 3$ A. c) Simulation results at $i_s = 6$ A. d) Experimental results at $i_s = 6$ A.

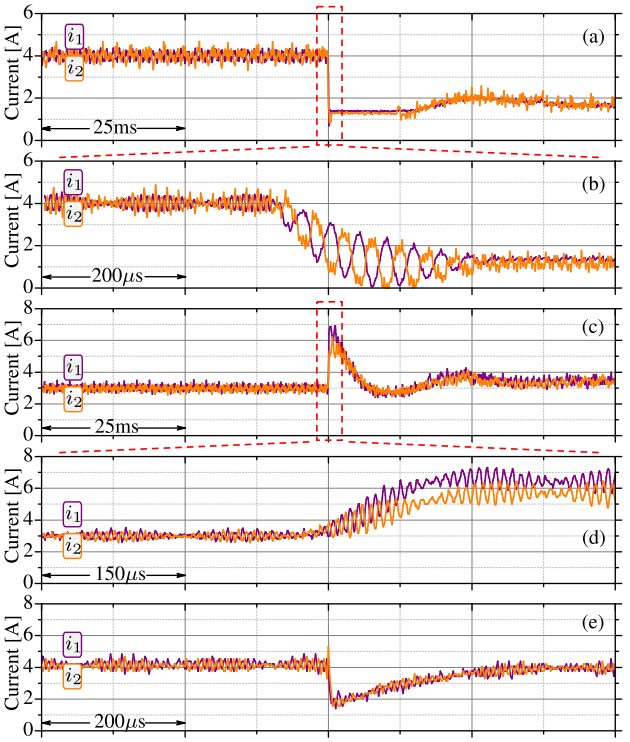

FIGURE 8. Experimental results of multi-phase LLC converters in a dynamic state. a) Step-down from 4 A to 2 A. b) Zoom response of graph (a). c) Step-up from 3 A to 4 A. d) Zoom response of graph (c). e) 50% of load disturbance.

controller adapts independently the frequency of each resonant converter. In this case frequencies are $f_{s1} = 62.5$ kHz and $f_{s2} = 55.5$ kHz.

Figure 7 illustrates the experimental and simulated currents in both resonant tanks. Despite the proposed multi-current scheme does not have a feed-back in the currents tanks, it balances the tanks currents as well as the output currents. The wave-forms of current tanks resemble as PSM because

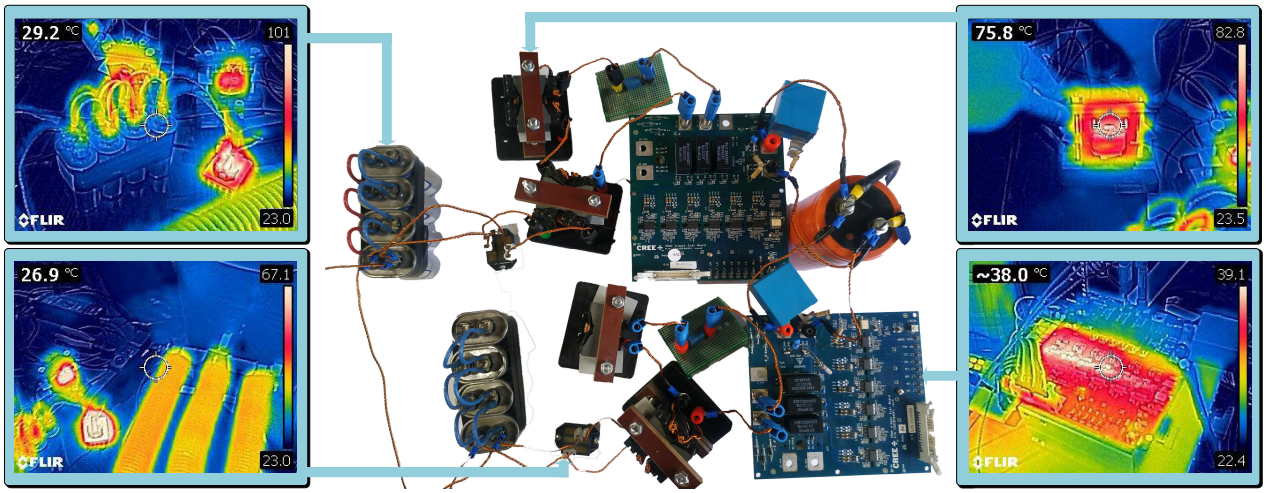

FIGURE 9. Experimental setup and thermal imagen of SiC inverter, resonant inductor, bridge diode and capacitors at steady state.

of angle-displacement currents, which is an effect caused by changing the working frequencies independently. It can be seen that both frequencies differ more at low output currents. Figure 7 (b) and Figure 7 (d) present a delay of 1μs and 0.3 μs, respectively. The big delay is done by boost mode while another is a consequence of the dead time of the gate driver board.

Figure 8 shows the dynamic performance of the proposed multi-current loop controller. Figure 8 (a)-(b) presents the output currents of both LLC converters under a step-down change on the current reference. The control moves the switching frequency around the resonant frequency to control the output current and to achieve current sharing. The control scheme achieves the current sharing also during the transient, showing dynamic stability. In the case of step-down, the response of the LLC converter has a negative transition with overshot and it is stabilized in 250 μs (Figure 8) (b). On the other hand, the caseμs of step-up shows a positive transition and also is stabilized at 250 μs (Figure 8) (d). Finally, Figure 8 (e) shows the control action when there is a 50% step-change in the load, reaching the steady-state in 200 μs approximately. These results support and evidence that multi-current control loops keep the balance of i_o in the multi-phase LLC resonant converter.

C. EFFICIENCY ANALYSIS

The efficiency was obtained through PLECS software using the experimental parameters of Table 1, the MOSFET model (CCS020M12CM2) and the passive component parameters from the manufacturers. The following power losses were taken into account: (i) E_{sw}: MOSFET turn-on and turn-off switching losses, (ii) E_{con}: MOSFET conduction losses; (iii) D_{loss}: diode reverse recovery losses; and (v) LC_{loss}: passive component losses (resonant capacitor, inductor and transformer). Figure 9 illustrates the experimental setup together with its thermal images, which are related to the power losses of the full-bridge and the tank, including the inductor and transformer.

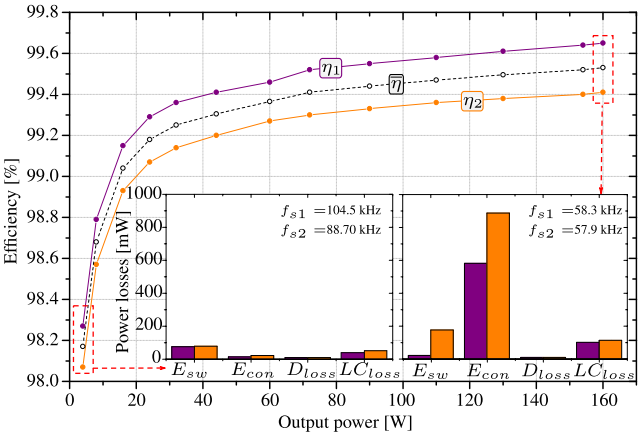

FIGURE 10. Efficiency curve of the multi-phase LLC converter using experimental setup ratings.

Figure 10 illustrates the efficiency curve operating the LLC converter at the experimental setup rating (V_{in} = 60 V). The switching power losses E_{sw} are low due to both converters are around their resonant frequencies, but in this case the losses are even lower than expected due to the low input voltage. The conduction losses E_{con} increases with the output power due to it is proportional to the output current. The efficiency increases with the output power, reaching the maximum efficiency at 160 W per LLC converter, where they are switching at f_{s1} = 58.3 kHz and f_{s2} = 57.9 kHz. On the other hand, the minimum efficiency is obtained at 2 W per LLC converter since LLC converters are switching at f_{s1} = 104.5 kHz and f_{s2} = 88.7 kHz. The LLC converter operates far above their resonant frequencies when it works at very low power, raising the switching losses.

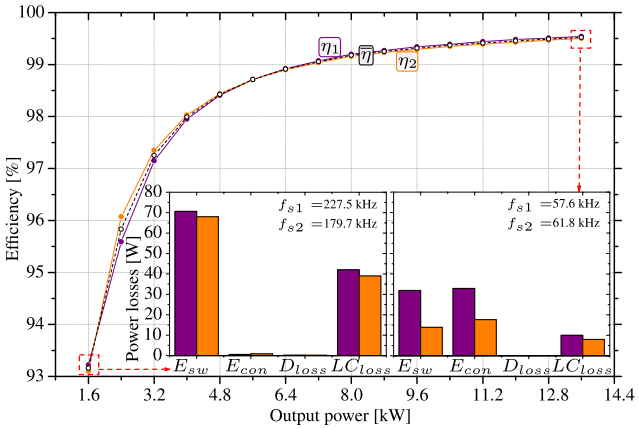

FIGURE 11. Efficiency curve of the multi-phase LLC converter using nominal ratings of SiC inverter module.

Figure 11 illustrates the efficiency curve operating the LLC converter at its nominal rating ($V_{in} = 1200$ V). The maximum efficiency is reached at 13.6 kW per LLC converter, switching at $f_{s1} = 57.6$ kHz and $f_{s2} = 61.8$ kHz. Both converters are near their resonance frequencies, reducing the switching losses but increasing the conduction losses E_{con} and the tank losses LC_{loss}. The minimum efficiency is obtained at 800 W per LLC converter, switching at $f_{s1} = 227.5$ kHz and $f_{s2} = 179.7$ kHz. The converters are far above their resonance frequencies, which highly increases the switching losses. However, the LLC converter was designed to operate at higher power ratings.

D. CURRENT SHARING ANALYSIS

The imbalance current at load in multi-phase LLC resonant converter is analyzed with the current sharing error (σ_L) [16], [20], [38], which is the difference between the output currents normalized:

$$\sigma_L = \left| \frac{I_1 - I_2}{I_1 + I_2} \right| \tag{19}$$

Figure 12 shows the current sharing error for the entire power range, presenting a higher error when the LLC converters have more current ripples. For instance, at 288 W the LLC converters have 2 A of current ripples and work at 59.8 kHz and 58.8 kHz. Anyway, the proposed multi-current control loop shows its capability of keeping the current sharing error in a value lower than 0.0005%.

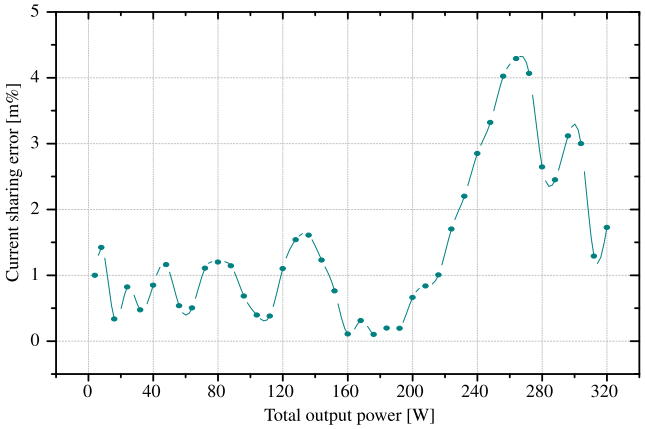

FIGURE 12. The unbalance current of the multi-phase LLC resonant converter with the multi-current control loop.

TABLE 2. Comparison between control loop proposed in [15] and the multi-current control loop proposed in this work.

	Control loop [15]	Control proposal
Load at 25%	$\sigma_L = 0.432\%$	$\sigma_L = 0.854\%$
Load at 45%	$\sigma_L = 0.451\%$	$\sigma_L = 0.015\%$
Load at 60%	$\sigma_L = 0.185\%$	$\sigma_L = 0.057\%$
Load at 98%	$\sigma_L = 0.033\%$	$\sigma_L < 0.001\%$
Shared information	Master-slave	Decentralized
Control modularity	Coupled controller	Decoupled PI controller
Complexity	Master-slave	Single current-loops

Table 2 shows a comparison between the proposed control and the control loop proposed in [15]. To carry out this comparison, the same parameters and operating points described in the reference were used, using four parallel converters in simulation. Both controls have very low current sharing error and the proposed control-loop presents even lower error at high power due to it was designed for nominal rating.

V. CONCLUSION

This paper proposed a simple decoupled control scheme for multi-phase LLC resonant converters using independent PI controllers to share the output currents evenly and to eliminate the circuiting current. The control scheme of each LLC converter uses the same output current reference, has identical PI controllers and implements pulse-frequency modulation (PFM) to obtain current sharing and eliminate circulating current, providing very low steady-state error and satisfactory transient performance, even under severe mismatch of the resonant tank parameters as well as disturbances on the load.

The proposed control scheme ensures the elimination of the dc component of the circulating currents, which is responsible for most of the avoidable power losses. Besides, it was demonstrated that under resonant tank mismatch, due to the nature of the converter, it is not possible to eliminate the ac and dc components of the circulating currents simultaneously, independently of the modulation used. However, an extensive analysis was presented for a better understanding of the modulation impact in the circulating current, which could be useful for future works such as the implementation of non-linear controllers.

Analytical and experimental assessments confirmed that the ripple of the output current cannot be eliminated under resonant tank mismatch, even by using interleave modulation. However, the proposed control scheme provides a reasonable trade-off between interleave and twin modulation. The multi-current control loop stands out by its high modularity, which is given by the non-dependence between control loops, the absence of cross measurements between converters and the same controller tuning for each regulator. Therefore,

the proposed multi-current control loop allows the use of multi-phase LLC resonant converters for high-current applications, such as fast chargers for electric vehicles, operating each unit with a simple PI controller and working close to the resonance frequency (f_s) to achieve soft switching in steady-state operation.

APPENDIX A
DESIGN OF THE GAPPED INDUCTOR AND THE TRANSFORMER

The first step in the design of the high-frequency inductors and transformers was the selection of material and type of cores. The SIFERRIT material N97 from TDK manufacturer was selected due to its suitable bandwidth for LLC tanks (Table 1). The PQ 50/50 core was chosen to reduce the transformer leakage inductance and get a uniform cross-sectional area at low volume. The inductors and primary side of transformers share the same current ($I_{max} = 8$A), so they use the same Litz wire, while the secondary side of the transformers uses a thicker wire because of the transformer ratio 2:1. The maximum inductance for the inductors and transformers is obtained by the air-gap length to change the core permeability and causing that the inductance value will have lower sensitivity to temperature, voltage, and frequency.

The minimum number of turns of the resonant inductors (N_{min}) and transformers (N_{min}^{prim}) are:

$$N_{min} = \frac{L_r \cdot I_{max}}{B_{max} \cdot A_e} \tag{20}$$

$$N_{min}^{prim} = \frac{V_{in}}{4 \cdot A_e \cdot B_{max} \cdot f} \tag{21}$$

where I_{max} is the maximum current and A_e is the effective area. The maximum magnetic flux density $B_{max} = 290$mT is obtained from the material hysteresis curve on its linear range at the temperature of 100 °C. Then N_{min} and N_{min}^{prim} are approximated to an integer number:

$$N = \begin{cases} \lceil N_{min} \rceil + 1 & \text{for inductor} \\ \lceil N_{min}^{prim} \rceil + 1 & \text{for transformer} \end{cases} \tag{22}$$

The air-gap g and the inductance factor A_L are used in the resonant inductors and transformers, they are obtained as:

$$A_L = L/N^2; \tag{23}$$

$$g = \frac{4\pi A_e}{10 A_L} \tag{24}$$

where $L = L_r$ for the resonant inductor and $L = L_m$ for the magnetizing inductance of the transformer. The manufacturer specifies that the A_L unit is [mH/$turn^2$] so L should use in [mH]. Finally, the number of turns on the secondary side of the transformer is:

$$N_{sec} = n \cdot N_{prim} \tag{25}$$

As a result of applying these equations, the parameters were obtained for the transformer and inductor in the table 3.

TABLE 3. Transformer and inductor parameters.

Parameter	L_{r1}	L_{r2}	L_{prim1}	L_{prim2}	L_{sec1}	L_{sec2}
N	19	21	26	25	13	13
g [mm]	0.66	0.66	0.66	0.66	0.66	0.66
n	-	-	2.1	1.9	-	-
L [μH]	221	243	398	365	105	105

APPENDIX B
TRANSFER FUNCTION OF THE OUTPUT CURRENT

To obtain the transfer function $G_{ifk}(s)$, a point of operation is selected to linearize the system. The LLC resonant converter can be described with its non-linearities as:

$$\frac{di_{L_{rk}}(t)}{dt} = \frac{1}{L_{rk}}(V_{in} - v_{C_{rk}}(t)) - \frac{n_k}{L_{rk}} \text{sign}(i_{L_{rk}}(t) - i_{L_{mk}}(t)) V_o(t) \tag{26}$$

$$\frac{dv_{ck}(t)}{dt} = \frac{1}{C_{rk}} i_{L_{rk}}(t) \tag{27}$$

$$\frac{di_{L_{mk}}(t)}{dt} = \frac{n_k}{L_{mk}} V_o \cdot \text{sign}(i_{L_{rk}}(t) - i_{L_{mk}}(t)) \tag{28}$$

$$\frac{dV_o(t)}{dt} = \frac{n_k}{C_{ok}} \left| i_{L_{rk}}(t) - i_{L_{mk}}(t) \right| - \frac{V_o(t)}{R_L} \tag{29}$$

The system is linearized in a state-space model $\dot{x} = Ax(t) + Bu(t)$, where the eigenvalues are analyzed. The more complex operation point of the LLC resonant converter is at resonant frequency due to the presence of a higher oscillation, overshoot and setting time [39]. Therefore, the LLC converter was linearized at the resonant frequency, using the small-signal model with average modeling, which results in the transfer function:

$$G_{vf_k}(s) = \frac{V_o(s)}{f_{sk}(s)} = \frac{k f_k}{s^2 \frac{L_{eq_k} C_{ok}}{n_k^2} + s \frac{L_{eq_k}}{R_L n_k^2} + 1} \tag{30}$$

The transfer function $G_{vf_k}(s)$ describes the relation between the output voltage and switching frequency and $V_o(s) = i_k(s)/(sC_{ok} + 1/R_L)$ is placed into $G_{vf_k}(s)$ for obtaining G_{if_k} in (4).

APPENDIX C
ZEROS AND POLES OF THE MULTI-CURRENT CONTROL LOOP

The zeros and poles of the whole system transfer function $G(s)$ are shown in Figure 4. To analyze the multi-current control loop $C_i(s)$ and the transfer function $G_{ifk}(s)$, the following equivalent transfer function is used:

$$G(s) = \frac{C_i(s) \cdot G_{if_k}(s)}{C_i(s) \cdot G_{if_k}(s) + 1} \tag{31}$$

$$G(s) = \frac{\kappa_k (sC_{ok} + \frac{1}{R_L})(s + Z_b)}{\left(s + \frac{1}{R_L} \cdot \frac{1}{C_{ok}+1}\right)\left(\frac{L_{eq_k}}{n_k^2} s^2 + (\kappa_k + 1)s + \kappa_k Z_b\right)} \tag{32}$$

$$Z_a = -\frac{1}{R_L} \cdot \frac{1}{C_{ok}} \tag{33}$$

$$P_r = -\frac{1}{R_L} \cdot \frac{1}{C_{ok} + 1} \tag{34}$$

$$P_j = -\frac{n_k^2}{2L_{eq_k}} \pm \frac{n_k^2}{2L_{eq_k}} \xi_{j_k} \tag{35}$$

$$\xi_{j_k} = \sqrt{(\kappa_k + 1)^2 - 4\left(\frac{L_{eq_k}}{n_k^2}\right)(\kappa_k Z_b)} \tag{36}$$

$G(s)$ has two zeros on the real negative axis Z_a and Z_b, where Z_a is defined by output capacitor C_{ok} and the load R_L. Next to Z_a is the P_r pole as shown in Figure 4. The zero Z_b is a degree of freedom to move the natural frequency (ω_k) of $G(s)$. The dominant poles P_j are conjugated and determined mainly by $k_p = \kappa_k / k_{f_k}$ because it changes the discriminant value (ξ_{j_k}), modifying the damping factor (ζ_k) of $G(s)$.

REFERENCES

[1] S. M. Tayebi, H. Hu, S. Abdel-Rahman, and I. Batarseh, "Dual-input single-resonant tank LLC converter with phase shift control for PV applications," *IEEE Trans. Ind. Appl.*, vol. 55, no. 2, pp. 1729–1739, Mar. 2019.

[2] T. S. Wable and V. M. Panchade, "Implementation on high-performance quasi-Z-source series resonant DC to DC converter for photovoltaic module level power electronics applications," in *Proc. Int. Conf. Commun. Electron. Syst. (ICCES)*, Jul. 2019, pp. 1358–1361.

[3] Y. Shen, H. Wang, Z. Shen, Y. Yang, and F. Blaabjerg, "A 1-MHz series resonant DC–DC converter with a dual-mode rectifier for PV microinverters," *IEEE Trans. Power Electron.*, vol. 34, no. 7, pp. 6544–6564, Jul. 2019.

[4] N. Shafiei, M. Ordonez, M. A. Saket Tokaldani, and S. A. Arefifar, "PV battery charger using an *L3C* resonant converter for electric vehicle applications," *IEEE Trans. Transport. Electrific.*, vol. 4, no. 1, pp. 108–121, Mar. 2018.

[5] R. N. M. de Oliveira, L. C. dos Santos Mazza, H. M. de Oliveira Filho, and D. D. S. Oliveira, "A three-port isolated three-phase current-fed DC–DC converter feasible to PV and storage energy system connection on a DC distribution grid," *IEEE Trans. Ind. Appl.*, vol. 55, no. 5, pp. 4910–4919, Sep. 2019.

[6] A. Chub, D. Vinnikov, E. Liivik, and T. Jalakas, "Multiphase quasi-Z-source DC–DC converters for residential distributed generation systems," *IEEE Trans. Ind. Electron.*, vol. 65, no. 10, pp. 8361–8371, Oct. 2018.

[7] C. Liu, X. Xu, D. He, H. Liu, X. Tian, Y. Guo, G. Cai, C. Ma, and G. Mu, "Magnetic-coupling current-balancing cells based input-parallel output-parallel (IPOP) LLC resonant converter modules for high-frequency isolation of DC distribution systems," *IEEE Trans. Power Electron.*, vol. 31, no. 10, pp. 6968–6979, Oct. 2016.

[8] S. A. Arshadi, M. Ordonez, W. Eberle, M. A. Saket, M. Craciun, and C. Botting, "Unbalanced three-phase *LLC* resonant converters: Analysis and trigonometric current balancing," *IEEE Trans. Power Electron.*, vol. 34, no. 3, pp. 2025–2038, Mar. 2019.

[9] R. Pandey and B. Singh, "A power-factor-corrected LLC resonant converter for electric vehicle charger using cuk converter," *IEEE Trans. Ind. Appl.*, vol. 55, no. 6, pp. 6278–6286, Nov. 2019.

[10] H.-N. Vu and W. Choi, "A novel dual full-bridge LLC resonant converter for CC and CV charges of batteries for electric vehicles," *IEEE Trans. Ind. Electron.*, vol. 65, no. 3, pp. 2212–2225, Mar. 2018.

[11] K. Shen, A. Tong, C. Shao, L. Hang, Y. He, Y. Zhang, G. Li, and J. Zhang, "ZVS control strategy of dual active bridge DC/DC converter with triple-phase-shift modulation considering RMS current optimization," *J. Eng.*, vol. 2019, no. 18, pp. 4708–4712, Jul. 2019.

[12] D. Sha, X. Wang, and D. Chen, "High-efficiency current-fed dual active bridge DC DC converter with ZVS achievement throughout full range of load using optimized switching patterns," *IEEE Trans. Power Electron.*, vol. 33, no. 2, pp. 1347–1357, Feb. 2018.

[13] S. Chakraborty and S. Chattopadhyay, "Fully ZVS, minimum RMS current operation of the dual-active half-bridge converter using closed-loop three-degree-of-freedom control," *IEEE Trans. Power Electron.*, vol. 33, no. 12, pp. 10188–10199, Dec. 2018.

[14] C. Fei, R. Gadelrab, Q. Li, and F. C. Lee, "High-frequency three-phase interleaved LLC resonant converter with GaN devices and integrated planar magnetics," *IEEE J. Emerg. Sel. Topics Power Electron.*, vol. 7, no. 2, pp. 653–663, Jun. 2019.

[15] S. Zong, H. Luo, W. Li, X. He, and C. Xia, "Theoretical evaluation of stability improvement brought by resonant current loop for paralleled LLC converters," *IEEE Trans. Ind. Electron.*, vol. 62, no. 7, pp. 4170–4180, Jul. 2015.

[16] H. Wang, Y. Chen, Y.-F. Liu, J. Afsharian, and Z. Yang, "A passive current sharing method with common inductor multiphase LLC resonant converter," *IEEE Trans. Power Electron.*, vol. 32, no. 9, pp. 6994–7010, Sep. 2017.

[17] B.-C. Kim, K.-B. Park, C.-E. Kim, and G.-W. Moon, "Load sharing characteristic of two-phase interleaved LLC resonant converter with parallel and series input structure," in *Proc. IEEE Energy Convers. Congr. Expo.* Sep. 2009, pp. 750–753.

[18] T. Guillod, D. Rothmund, and J. W. Kolar, "Active magnetizing current splitting ZVS modulation of a 7 kV/400 v DC transformer," *IEEE Trans. Power Electron.*, vol. 35, no. 2, pp. 1293–1305, Feb. 2020.

[19] M. A. Shamshuddin, F. Rojas, R. Cardenas, J. Pereda, M. Diaz, and R. Kennel, "Solid state transformers: Concepts, classification, and control," *Energies*, vol. 13, no. 9, p. 2319, May 2020.

[20] H. Wang, Y. Chen, and Y.-F. Liu, "A passive-impedance-matching technology to achieve automatic current sharing for a multiphase resonant converter," *IEEE Trans. Power Electron.*, vol. 32, no. 12, pp. 9191–9209, Dec. 2017.

[21] H. Wang, Y. Chen, Y. Qiu, P. Fang, Y. Zhang, L. Wang, Y.-F. Liu, J. Afsharian, and Z. Yang, "Common capacitor multiphase LLC converter with passive current sharing ability," *IEEE Trans. Power Electron.*, vol. 33, no. 1, pp. 370–387, Jan. 2018.

[22] Y. Yang, J. Yao, H. Li, and J. Zhao, "A novel current sharing method by grouping transformer's secondary windings for a multiphase LLC resonant converter," *IEEE Trans. Power Electron.*, vol. 35, no. 5, pp. 4877–4890, May 2020.

[23] M. Noah, K. Umetani, J. Imaoka, and M. Yamamoto, "Lagrangian dynamics model and practical implementation of an integrated transformer in multi-phase LLC resonant converter," *IET Power Electron.*, vol. 11, no. 2, pp. 339–347, Feb. 2018.

[24] M. Noah, S. Endo, H. Ishibashi, K. Nanamori, J. Imaoka, K. Umetani, and M. Yamamoto, "A current sharing method utilizing single balancing transformer for a multiphase LLC resonant converter with integrated magnetics," *IEEE J. Emerg. Sel. Topics Power Electron.*, vol. 6, no. 2, pp. 977–992, Jun. 2018.

[25] W.-J. Gu and K. Harada, "A new method to regulate resonant converters," *IEEE Trans. Power Electron.*, vol. 3, no. 4, pp. 430–439, Oct. 1988.

[26] Z. Hu, Y. Qiu, L. Wang, and Y.-F. Liu, "An interleaved LLC resonant converter operating at constant switching frequency," *IEEE Trans. Power Electron.*, vol. 29, no. 6, pp. 2931–2943, Jun. 2014.

[27] E. Orietti, P. Mattavelli, G. Spiazzi, C. Adragna, and G. Gattavari, "Current sharing in three-phase LLC interleaved resonant converter," in *Proc. IEEE Energy Convers. Congr. Expo.*, Sep. 2009, pp. 1145–1152.

[28] J. Jang, S. Choi, B. Choi, and S. Hong, "Average current mode control to improve current distributions in multi-module esonant DC-to-DC converters," in *Proc. 8th Int. Conf. Power Electron. ECCE Asia*, May 2011, pp. 2312–2319.

[29] K. Murata and F. Kurokawa, "An interleaved PFM LLC resonant converter with phase-shift compensation," *IEEE Trans. Power Electron.*, vol. 31, no. 3, pp. 2264–2272, Mar. 2016.

[30] H. Figge, T. Grote, N. Froehleke, J. Boecker, and P. Ide, "Paralleling of LLC resonant converters using frequency controlled current balancing," in *Proc. IEEE Power Electron. Spec. Conf.*, Jun. 2008, pp. 1080–1085.

[31] Y. Wang, X. Ren, Z. Zhang, and Q. Chen, "Research on current sharing strategy of parallel LLC resonant converter," in *Proc. IEEE Appl. Power Electron. Conf. Expo. (APEC)*, Mar. 2019, pp. 2294–2299.

[32] M. Frivaldsky, P. Spanik, J. Morgos, and M. Pridala, "Control strategy proposal for modular architecture of power supply utilizing LCCT converter," *Energies*, vol. 11, no. 12, p. 3327, Nov. 2018.

[33] B. C. Hyeon and B. H. Cho, "Multiple output of dual half bridge LLC resonant converter using PFM-PD control," in *Proc. IEEE Energy Convers. Congr. Expo.*, Sep. 2009, pp. 1133–1140.

[34] S. Saggini, R. Rizzolatti, M. Ursino, and O. Zambetti, "380v digital isolated quasi-resonant multiphase converter for high power LED application," in *Proc. IEEE Appl. Power Electron. Conf. Expo. (APEC)*, Mar. 2018, pp. 3459–3465.

[35] R. Beiranvand, B. Rashidian, M. R. Zolghadri, and S. M. Hossein Alavi, "A design procedure for optimizing the LLC resonant converter as a wide output range voltage source," *IEEE Trans. Power Electron.*, vol. 27, no. 8, pp. 3749–3763, Aug. 2012.
[36] R. Beiranvand, B. Rashidian, M. R. Zolghadri, and S. M. H. Alavi, "Using LLC resonant converter for designing wide-range voltage source," *IEEE Trans. Ind. Electron.*, vol. 58, no. 5, pp. 1746–1756, May 2011.
[37] Z. Fang, T. Cai, S. Duan, and C. Chen, "Optimal design methodology for LLC resonant converter in battery charging applications based on time-weighted average efficiency," *IEEE Trans. Power Electron.*, vol. 30, no. 10, pp. 5469–5483, Oct. 2015.
[38] O. Kirshenboim and M. M. Peretz, "Combined multilevel and two-phase interleaved LLC converter with enhanced power processing characteristics and natural current sharing," *IEEE Trans. Power Electron.*, vol. 33, no. 7, pp. 5613–5620, Jul. 2018.
[39] F. Degioanni, I. G. Zurbriggen, and M. Ordonez, "Dual-loop controller for LLC resonant converters using an average equivalent model," *IEEE Trans. Power Electron.*, vol. 33, no. 11, pp. 9875–9889, Nov. 2018.

MARTIN MORENO (Student Member, IEEE) received the B.Eng. degree in mechatronics engineering from the Technological Institute of Querétaro, Querétaro, Mexico, in 2015, and the master's degree (Hons.) in advanced technology from the National Polytechnic Institute, Mexico City, Mexico, in 2017, where he is currently pursuing the Ph.D. degree in advanced technology. Since 2018, he has been a Ph.D. Exchange Student with the Power and Energy Conversion Laboratory, Pontifical Catholic University of Chile, Santiago, Chile. His research interests include resonant converter topologies and control schemes for high-frequency power converters.

JAVIER PEREDA (Member, IEEE) received the B.Sc. (Eng.) degree (Hons.) in electrical engineering, and the M.Sc. and Ph.D. degrees in electrical engineering all from the Pontifical Catholic University of Chile, Santiago, Chile, in 2009 and 2013, respectively. He has been an Assistant Professor with the Department of Electrical Engineering, Pontificia Universidad Católica de Chile, since 2013. From 2014 to 2016, he was an Associate Research of the Control and Power Group, Department of Electrical and Electronic Engineering, Imperial College London. He is currently an Associate Research of the Solar Energy Research Center, Chile, and the UC Energy Research Center, Chile. He is also the Principal Investigator of the Electric Vehicle Laboratory and the Power and Energy Conversion Laboratory (PEClab), Pontificia Universidad Católica de Chile. His research interests include power electronics and control applied to electric vehicles, ac and dc electric networks, microgrids, renewable energy, multilevel converters, industrial applications, and motor drives.

FELIX ROJAS (Member, IEEE) was born in Santiago, Chile. He received the B.Eng. and M.Sc. degrees (Hons.) in electrical engineering from the Universidad de Santiago de Chile, Santiago, in 2009, and the Ph.D. degree in electrical engineering from the Technical University of Munich, Munich, Germany, in 2016. He is currently an Associate Professor of Electrical Engineering with the Universidad de Santiago de Chile. He is also the Head of the Electrical Energy Technologies Research Center (E2TECH), USACH. He is also an Associate Research with the Solar Energy Research Center (SERC Chile). His research interests include in control of modular multilevel converters, solid state transformers, renewable energy conversion, electric vehicles chargers, and machine drives.

IVAN DOMINGUEZ-LOPEZ received the master's degree and the Ph.D. degree in sciences from the National Autonomous University of Mexico (UNAM). He has worked with the UNAM's Institute of Physics, the National Metrology Center, and the National Polytechnic Institute of Mexico, in addition to having carried out research stays at the Berkeley National Laboratory, the University of Nevada, USA, and at the Physikalisch-technische bundesanstalt, Germany. Since 2005, he has been working as a full-time Researcher with CICATA-IPN Querétaro, where he also teaches postgraduate classes. He is currently a Physicist. He has conducted research in different fields: atomic physics, time and frequency metrology, materials processing and manufacturing, tribology, and instrumentation.